https://doi.org/10.2352/ISSN.2470-1173.2020.10.IPAS-181

Non-Blind Image Deconvolution Based on "Ringing" Removal Using Convolutional Neural Network

Takahiro Kudo, Takanori Fujisawa, Takuro Yamaguchi, Masaaki Ikehara; Keio University; Yokohama, Kanagawa, Japan

Abstract

Image deconvolution has been an important issue recently. It has two kinds of approaches: non-blind and blind. Non-blind deconvolution is a classic problem of image deblurring, which assumes that the PSF is known and does not change universally in space. Recently, Convolutional Neural Network (CNN) has been used for non-blind deconvolution. Though CNNs can deal with complex changes for unknown images, some CNN-based conventional methods can only handle small PSFs and does not consider the use of large PSFs in the real world. In this paper we propose a non-blind deconvolution framework based on a CNN that can remove large scale ringing in a deblurred image. Our method has three key points. The first is that our network architecture is able to preserve both large and small features in the image. The second is that the training dataset is created to preserve the details. The third is that we extend the images to minimize the effects of large ringing on the image borders. In our experiments, we used three kinds of large PSFs and were able to observe high-precision results from our method both quantitatively and qualitatively.

Introduction

Image deblurring has been an important issue recently because of the increasing number of imaging devices and the spread of HD displays. Thus, the demand for image blurring with high accuracy has increased in the past several years. [1] In many cases, image blur is caused by the motion of the camera and the subject, failure to focus all view fields, etc.

Image deconvolution has two kinds of approaches: non-blind and blind. Non-blind deconvolution is a classic image processing problem which assumes that the blur kernel (PSF) is known and doesn't change universally in space. In contrast, blind deconvolution first estimates the PSF and then removes the blur based on non-blind methods. The improvement of this algorithms is important for image deblurring.

The most common method for deconvolution is the Wiener Filter [2] which minimizes the mean square error between the estimated image and the target image. Another common method is the Richardson-Lucy (R-L) method [3]. This method is processed iteratively to move the ratio between the observed image and the initial true image closer to 1. Although these methods are efficient for non-blind deconvolution, they are known to produce deconvolution artifacts in images known as "ringing". This rippling effect is caused by the edges and ends of the blurred image and has a negative impact on the output image. Therefore, several methods have been proposed to minimize the ringing effect, such as Krishnan *et al.* [4], Levin *et al.* [5], and EPLL [6].

Recently, Convolutional Neural Network (CNN) has been used for many image processing tasks such as super-resolution [7, 8], denoising [9], etc. CNNs are able to flexibly deal with complex changes in images and has been used for image deconvolution. Schuler *et al.* [10] first used a MLP for image deconvolution. Moreover, Son *et al.* [11] proposed a CNN-based framework which handles several PSFs. Although both methods perform very well on small PSFs, they are not able to effectively handle larger kernels. Furthermore, both methods only take into account the ideal circumstance and don't consider the large ringing effect in the output image.

In this paper, we propose a non-blind deconvolution framework based on a CNN. First, the blurred image is deblurred with the R-L method [3] which results in a deblurred image with ringing effects. The ringing effect is then eliminated by a CNN trained through residual learning. The final image is generated via post-processing.

Out proposed method has three key points. One is our unique CNN architecture that is able to preserve both small and large features in images. The network used 3×3, 5×5, and 7×7 convolution layers which is able to remove large ringing artifacts while retaining the details. Another point is our training dataset which is devised to maintain the details. It contains patches with smaller ringing effects so that the CNN learns the differences between the minute ringing artifacts and the details. The final point is the use of image extension to reduce the influence of large ringing effects.

In our experiments, we used three kinds of large PSFs: straight kernel, polyline kernel, and complex kernel. When testing our model, we were able to observe high-precision results both objectively and subjectively.

Related Works

The Problem of Image Deconvolution

Image convolution is defined by the following equation as

$$\boldsymbol{y} = \boldsymbol{x} \otimes \boldsymbol{k} + \boldsymbol{n} \tag{1}$$

where $\boldsymbol{y}$ is the blurred image, $\boldsymbol{x}$ is the original image, $\boldsymbol{k}$ is the blur kernel (PSF), and $\boldsymbol{n}$ is additive noise. Non-blind deconvolution is the problem of solving for $\boldsymbol{x}$ given $\boldsymbol{k}$. In this paper, we assume that $\boldsymbol{n} = \boldsymbol{0}$ to clearly observe the performance of the proposed image deconvolution method.

The non-CNN Based Conventional Algorithms

The most common conventional method is the Wiener Filter. [2]. First, the Fourier transform of (1) is

$$Y = X \cdot K \tag{2}$$

where Y, X, K are the Fourier transform of $\boldsymbol{y}, \boldsymbol{x}, \boldsymbol{k}$. Solving for $\boldsymbol{x}$ results in, the Wiener Filter is used as

$$\boldsymbol{x} = \mathscr{F}^{-1}\left(\frac{Y}{K}\right) \simeq \mathscr{F}^{-1}\left(Y \cdot \frac{K}{K^2 + \Gamma}\right) \tag{3}$$

where Γ is an extremely small value to prevent the equation from diverging in the case of $K = 0$.

Another common method is the Richardson-Lucy (R-L) method [3]. This method first estimates the initial true image $\boldsymbol{x}^{(1)}$ and moves the ratio of $\boldsymbol{y}$ to $\boldsymbol{x}^{(1)} \otimes \boldsymbol{k}$ closer to 1. This is done in an iterative process,

$$\boldsymbol{x}^{(t+1)} = \boldsymbol{x}^{(t)} \circ \left(\frac{\boldsymbol{k}^* \otimes \boldsymbol{y}}{\boldsymbol{k} \otimes \boldsymbol{x}^{(t)}} \right) \tag{4}$$

where $\boldsymbol{x}^{(t)}$ is the image deconvolved t times and $\boldsymbol{k}^*$ is the transposed matrix of $\boldsymbol{k}$. The parameter t is assigned by users. Other methods for non-blind deconvolution include Krishnan *et al.* [4], Levin *et al.* [5], and EPLL [6].

The CNN Based Conventional Algorithms

Recently, CNN-based algorithms have been proposed for image processing tasks since CNNs are able to deal with complex changes for unknown images fluently. For the non-blind deconvolution task, MLP (multi-layer perceptron) proposed by Schuler *et al.* [10], and Son *et al.* [11] are proposed. Both methods use the Wiener Filter first to get the preprocessing image $\boldsymbol{x}'$. They then generate the estimated image from a CNN,

$$\boldsymbol{x} = F_{\boldsymbol{\theta}}(\boldsymbol{x}') \tag{5}$$

where $\boldsymbol{\theta}$ is the weight of the convolution layers, batch-normalization layers, and biases in the CNN. The network learns the optimal parameters $\boldsymbol{\theta}$ from the given dataset by minimizing the mean square error between the target image $\boldsymbol{x}$ and the estimated image $\boldsymbol{x}'$,

$$\boldsymbol{\theta} = \underset{\boldsymbol{\theta}}{\operatorname{argmin}} \sum_{p=1}^{P} \|\boldsymbol{x}_p - F_{\boldsymbol{\theta}}(\boldsymbol{x}'_p)\|_2^2 \tag{6}$$

where p is the batch number and P is the total number of batches. The MLP method [10] uses a network with four hidden layers where it takes patches of size 39×39 as input and outputs a patch of size 13×13. In contrast, Son *et al.* [11] has long and short skip-connections for long-term memory effects and captures small changes.

Proposed Method

The Problems of the Conventional Methods

These non-CNN based and CNN based methods have several problems. Although the Wiener Filter [2] and the R-L method [3] are very efficient for non-blind deconvolution, they can produce deconvolution artifacts, called "ringing", in the output image. Compared to these two methods, other non-CNN based methods [4–6], are able to reduce the ringing effects but at the cost of some blur remaining in the output image. This is because the reduction in ringing artifacts are correlated to the deblurring accuracy.

The CNN-based methods [10, 11] solve these problems in non-CNN based methods mentioned above. However, they may not handle handle large sizes of the kernel $\boldsymbol{k}$. Moreover, these methods only consider the ideal situation in which the ringing effects generated by the borders of $\boldsymbol{y}$ are nonexistent by using the "circular" convolution of $\boldsymbol{x}$ and $\boldsymbol{k}$. The circular convolution assumes that the y is periodic without the considering the boundaries of the image. In Fig. 1, the blurred image generated by a circular convolution with a straight kernel is processed very well. In contrast, the blurred image generated by a normal convolution is not processed very well, resulting in ringing effects. Thus, these methods do not take into consideration the effects of the boundaries of $\boldsymbol{y}$ when seeking $\boldsymbol{x}$.

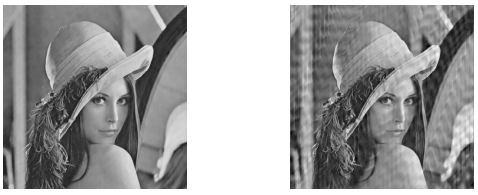

(a) Circular (b) Not Circular

Figure 1. The deconvolution images by [11], before processed by "Circular" and "Not Circular" convolution

The Flow of the Proposed Method

In order to solve the problems evident in the conventional methods, we propose a new method that can handle a large $\boldsymbol{k}$ and remove the ringing artifacts generated by the borders of $\boldsymbol{y}$.

The flow of the proposed method is represented below. First, the R-L method [3] is used as shown in (4), resulting in a deblurred image $\boldsymbol{x}'$. This method is very efficient for non-blind image deconvolution but results in larger ringing effects than other methods. Second, the CNN is used to remove the ringing artifacts present in $\boldsymbol{x}'$. Finally, the postprocessing of [11] is used to preserve very small details in the image.

The CNN used in our method is trained by a residual dataset. This dataset is composed of pairs $\boldsymbol{x}'$ and ringing components $\boldsymbol{r} = \boldsymbol{x}' - \boldsymbol{x}$. We use this sort of dataset since residual learning has proved to result in high accuracy in conventional methods such as DnCNN [9], VDSR [12]. The parameters $\boldsymbol{\theta}$ in our network is trained to minimize the following.

$$\boldsymbol{\theta} = \underset{\boldsymbol{\theta}}{\operatorname{argmin}} \sum_{p=1}^{P} \|\boldsymbol{x}'_p - \boldsymbol{x}_p - F_{\boldsymbol{\theta}}(\boldsymbol{x}'_p)\|_2^2. \tag{7}$$

Next, we explain the three points of the method.

The Points of the Proposed Method

Unique Network Architecture

The first point is that our unique network architecture as shown in Fig. 2. In ringing removal, it is known that a large kernel in a convolution layer is most effective in removing large ringing effects. In contrast, a smaller kernel is more effective in removing smaller ringing effects and is better able to preserve the details. Therefore, we propose three parallel networks with varying kernel sizes of 7×7, 5×5, 5×5.

In Fig. 2, one of the parallel networks can be expressed as

$$\begin{aligned} \boldsymbol{z}_1 &= \phi(\boldsymbol{W}_1 * \boldsymbol{x}' + \boldsymbol{b}_1) \\ \boldsymbol{z}_l &= \phi(\mathrm{BN}(\boldsymbol{W}_l * \boldsymbol{z}_{l-1} + \boldsymbol{b}_l)), \ \ 2 \le l \le L \end{aligned} \tag{8}$$

where $\boldsymbol{W}_l$ and $\boldsymbol{b}_l$ are trained parameters, BN is the Batch Nomalization layer [13] to speed up training and improve the accuracy, ϕ is the Leaky Rectified Linear Unit [14], $*$ is the convolution operation. $\boldsymbol{z}_l$ is the output of the l-th layer. At the end of the 7×7

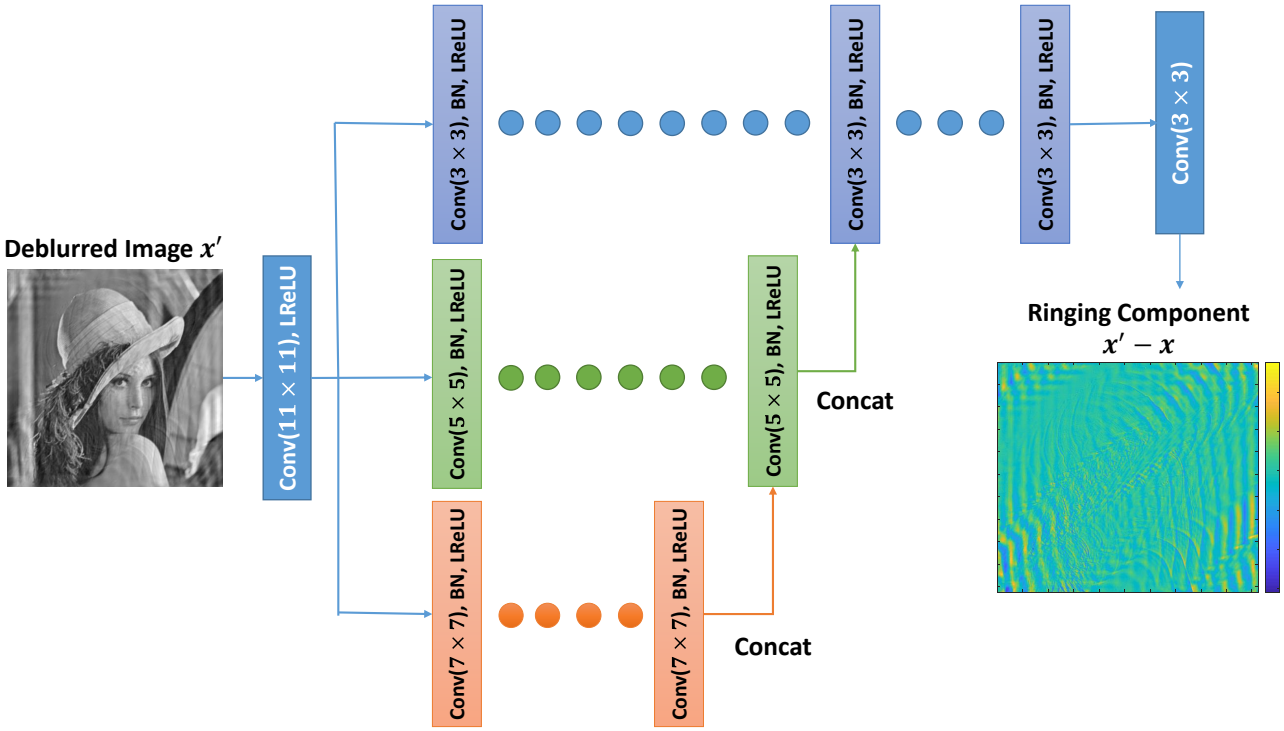

Figure 2. The Proposed Network Architecture

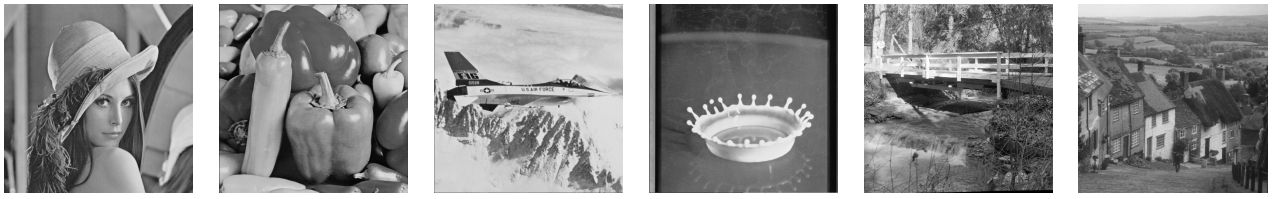

(a) Lena (b) Pepper (c) Airplane (d) Milkdrop (e) Bridge (f) Goldhill

Figure 3. The standard grayscale test images

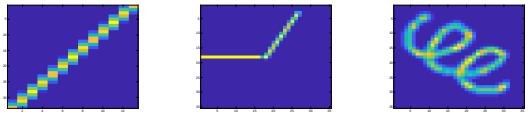

(a) Straight (b) Polyline (c) Complex

Figure 4. The three kinds of kernels for the experiment

convolution linear network, the z_L is concatenated to the $(L+1)$-th 5×5 convolution layer. The output of the 7×7 convolution network z_l is concatenated with the output of the 5×5 one. Likewise, the output of the 5×5 convolution network is concatenated with 3×3 convolution network. This architecture makes it possible for the CNN to remove large ringing artifacts while retaining desirable details.

The Devised Training Datasets

The second point is that we create the training dataset with the aim of maintaining details in the output image. The data pairs $\{x', r\}$ in the dataset have the following relationship.

$$r = x' - x. \tag{9}$$

The dataset of x'' is expressed with a weak ringing component r_s,

$$r_s = r \cdot s,\ 0 < s \leq 1$$
$$x'' = x + r_s \tag{10}$$

where s is a parameter for making the weak ringing datasets $\{x'', r_s\}$. We prepare three datasets: $\{x', r_{s=1}\}, \{x'', r_{s=3/4}\}, \{x''', r_{s=1/2}\}$. Preparing these datasets with varying ringing sizes forces the CNN to learn the different between r_s and the details.

Image Extension

The third point is minimizing the effects of large ringing artifacts by image extension. In the overall framework of the proposed method, y is enlarged by 10 pixels on all 4 sides symmetrically before using the R-L method [3]. Next, the ringing artifacts are removed. Finally, the borders of x' is cut by 10 pixels. This reduces the effect of ringing artifacts.

(a) Original image (b) Blurred image (c) Krishnan *et al.* [4] (d) Levin *et al.* [5]

(e) EPLL [6] (f) MLP [10] (g) Son *et al.* [11] (h) Proposed

Figure 5. The subjective comparison on the "Lena" image blurred by the polyline kernel, same as Fig. 4(b)

Table 1
THE MESUREMENT RESULTS OF THREE KERNELS (PSNR(DB)/SSIM)

(a) The straight kernel

Images	Krishnan *et al.* [4]	Levin *et al.* [5]	EPLL [6]	MLP [10]	Son *et al.* [11]	Proposed
Lena	27.54 / 0.795	28.95 / 0.815	28.47 / 0.855	26.08 / 0.757	27.09 / 0.799	**31.17 / 0.887**
Pepper	27.14 / 0.779	27.84 / 0.789	25.79 / 0.810	22.31 / 0.642	24.05 / 0.700	**28.08 / 0.833**
Airplane	26.05 / 0.810	26.09 / 0.810	27.30 / **0.862**	24.78 / 0.756	27.04 / 0.794	**28.03** / 0.859
Milkdrop	28.52 / 0.826	30.32 / 0.845	23.31 / 0.835	27.15 / 0.787	27.55 / 0.802	**31.32 / 0.886**
Bridge	21.77 / 0.484	22.46 / 0.508	23.35 / 0.623	20.87 / 0.572	23.21 / **0.781**	**24.93** / 0.779
Goldhill	26.23 / 0.636	26.80 / 0.652	27.10 / 0.720	22.28 / 0.618	23.89 / 0.788	**28.56 / 0.830**

(b) The polyline kernel

Images	Krishnan *et al.* [4]	Levin *et al.* [5]	EPLL [6]	MLP [10]	Son *et al.* [11]	Proposed
Lena	27.75 / 0.829	29.98 / 0.839	28.60 / 0.876	27.67 / 0.817	28.93 / 0.887	**31.79 / 0.905**
Pepper	27.54 / 0.821	29.92 / 0.831	24.02 / 0.822	27.13 / 0.792	27.97 / 0.861	**30.06 / 0.872**
Airplane	25.76 / 0.858	28.19 / 0.870	26.80 / 0.891	28.95 / 0.874	30.53 / 0.913	**30.60 / 0.924**
Milkdrop	27.88 / 0.858	30.24 / 0.870	24.87 / 0.860	28.87 / 0.810	27.55 / 0.801	**30.11 / 0.895**
Bridge	23.81 / 0.640	24.62 / 0.654	24.07 / 0.731	24.59 / 0.701	**26.77 / 0.870**	25.28 / 0.824
Goldhill	27.08 / 0.741	28.64 / 0.752	28.49 / 0.806	26.51 / 0.743	27.62 / **0.870**	**29.57** / 0.859

(c) The complex kernel

Images	Krishnan *et al.* [4]	Levin *et al.* [5]	EPLL [6]	MLP [10]	Son *et al.* [11]	Proposed
Lena	27.02 / 0.769	28.09 / 0.791	28.75 / 0.850	26.57 / 0.782	27.06 / 0.833	**29.82 / 0.869**
Pepper	26.24 / 0.753	27.41 / 0.777	26.01 / 0.803	25.10 / 0.738	25.28 / 0.772	**27.87 / 0.808**
Airplane	25.01 / 0.779	25.83 / 0.800	27.10 / 0.866	27.10 / 0.842	**28.28 / 0.879**	28.11 / 0.874
Milkdrop	25.01 / 0.779	**29.62** / 0.837	26.71 / 0.838	26.80 / 0.773	26.26 / 0.777	28.20 / **0.843**
Bridge	22.28 / 0.473	22.61 / 0.484	23.68 / 0.642	22.98 / 0.642	24.52 / **0.835**	**25.19** / 0.780
Goldhill	25.92 / 0.626	26.52 / 0.639	27.76 / 0.736	24.42 / 0.661	24.88 / 0.776	**28.42 / 0.808**

(a) Original image (b) Blurred image (c) Krishnan *et al.* [4] (d) Levin *et al.* [5]

(e) EPLL [6] (f) MLP [10] (g) Son *et al.* [11] (h) Proposed

Figure 6. The subjective comparison on the "Goldhill" image blurred by the complex kernel, same as Fig. 4(c)

Training

We use Adam [15] to minimize the objective function in (7). We start with a learning rate of 0.001 and multiply is by 0.1 every 10 epochs. A mini-batch size is set to 64 and the total number of epochs is 50. To make the dataset, we randomly chose 500 images from the Microsoft COCO dataset [16] and converted it to grayscale images $\boldsymbol{x}$. We then convolved the 30×30 the straight $\boldsymbol{k}$ and iterate the R-L method [3] 30 times to create $\boldsymbol{x}'$. We also created three datasets as shown in (10). Furthermore, we increase the dataset by rotating the kernel $\boldsymbol{k}$ by an angle every 15 degrees between 0 and 180. The number of the $\{3 \times 3, 5 \times 5, 7 \times 7\}$ convolution layers is respectively $\{20,15,10\}$. The patch size is set as 99×99, and 300 thousand patches are used for training.

Experimental Results

In this section, we show the results of testing on the six standard grayscale images of SIDBA (Standard Image Data-BAse) [17] such as "Lena", "Pepper", "Airplane", "Milkdrop", "Bridge", and "Goldhill". These images were not used in the training dataset and are shown in Fig. 3. The size of the images is 512×512. We compare the proposed method with the non-CNN based methods (Krishnan *et al.* [4], Levin *et al.* [5], EPLL [6]) and the CNN based methods (MLP [10] and Son *et al.* [11]). This was implemented in MATLAB with the source codes that the authors provided.

How to Experiment

In the experiments, we set the convolution between $\boldsymbol{x}$ and $\boldsymbol{k}$ as 'symmetric', not 'circular'. We set the parameters of the conventional methods fixed and the number of iterations of the R-L method of the proposed method is set to 40. We used three types of $\boldsymbol{k}$ as shown in Fig. 4 for the experiments. The Fig. 4(a) is the straight motion kernel whose angle is 70 degree, the Fig. 4(b) is the Polyline whose angles are 60 and 180 degree, and the Fig. 4(c) is the complex kernel. We evaluate the results objectively with PSNR and SSIM values, and subjectively to compare each method.

The Results of the Experiments

From Table 1, we can see that our method performs the best objectively with the highest PSNR and SSIM values in most cases. In particular, our method produces high values in Table 1(b) and 1(c) in spite of training the network with datasets created from only the straight PSF. To compare the performance of the methods subjectively, we give some examples of restored images in Figs. 5-6. As shown in Figs. 5(c)-5(d) and 6(c)-6(d), the conventional methods do not perform well. When comparing the images in Figs. 5(f)-5(g) and 6(f)-6(g) to images in Figs. 5(c)-5(d) and 6(c)-6(d), it is obvious that the CNN-based methods are better for preserving the details. However, strong ringing artifacts still remain in the restored images. In Figs. 5(e) and 6(e), the ringing artifacts are removed, but the details are removed from the images. In contrast, Figs. 5(h) and 6(h), show that the proposed method removes the ringing effect while preserving the details clearly.

Conclusion

In this paper, we propose a new method for non-blind image deconvolution. Our experiments show that our method is superior compared to the conventional methods in several cases. However, there still are cases where the conventional methods outperform the proposed method. It is believed that these cases are caused by

either the R-L method [3] or the size of the dataset.

References

[1] J. Flusser, S. Farokhi, C. Höschl, T. Suk, B. Zitová, and M. Pedone, "Recognition of images degraded by gaussian blur," *IEEE Transactions on Image Processing*, vol. 25, no. 2, pp. 790–806, 2016.

[2] N. Wiener, "Extrapolation, inerpolation, and smoothing of stationary time series," 1975.

[3] W. H. Richardson, "Bayesian-based iterative method of image restoration," *JOSA*, vol. 62, no. 1, pp. 55–59, 1972.

[4] D. Krishnan and R. Fergus, "Fast image deconvolution using hyper-laplacian priors," in *Advances in neural information processing systems*, 2009, pp. 1033–1041.

[5] A. Levin, R. Fergus, F. Durand, and W. T. Freeman, "Deconvolution using natural image priors," *Massachusetts Institute of Technology, Computer Science and Artificial Intelligence Laboratory*, vol. 3, 2007.

[6] D. Zoran and Y. Weiss, "From learning models of natural image patches to whole image restoration," in *2011 International Conference on Computer Vision*. IEEE, 2011, pp. 479–486.

[7] C. Dong, C. C. Loy, K. He, and X. Tang, "Image super-resolution using deep convolutional networks," *IEEE transactions on pattern analysis and machine intelligence*, vol. 38, no. 2, pp. 295–307, 2016.

[8] Y. Yoon, H.-G. Jeon, D. Yoo, J.-Y. Lee, and I. S. Kweon, "Light-field image super-resolution using convolutional neural network," *IEEE signal processing letters*, vol. 24, no. 6, pp. 848–852, 2017.

[9] K. Zhang, W. Zuo, Y. Chen, D. Meng, and L. Zhang, "Beyond a gaussian denoiser: Residual learning of deep cnn for image denoising," *IEEE Transactions on Image Processing*, vol. 26, no. 7, pp. 3142–3155, 2017.

[10] S. Christian, B. Harold, Christopher, H. Stefan, and S. Bernhard, "A machine learning approach for non-blind image deconvolution," in *2013 IEEE Conference on Computer Vision and Pattern Recognition*, June 2013, pp. 1067–1074.

[11] H. Son and S. Lee, "Fast non-blind deconvolution via regularized residual networks with long/short skip-connections," in *2017 IEEE International Conference on Computational Photography (ICCP)*, May 2017, pp. 1–10.

[12] J. Kim, J. Kwon Lee, and K. Mu Lee, "Accurate image super-resolution using very deep convolutional networks," in *Proceedings of the IEEE conference on computer vision and pattern recognition*, 2016, pp. 1646–1654.

[13] S. Ioffe and C. Szegedy, "Batch normalization: Accelerating deep network training by reducing internal covariate shift," *arXiv preprint arXiv:1502.03167*, 2015.

[14] A. L. Maas, A. Y. Hannun, and A. Y. Ng, "Rectifier nonlinearities improve neural network acoustic models," in *Proc. icml*, vol. 30, no. 1, 2013, p. 3.

[15] D. P. Kingma and J. Ba, "Adam: A method for stochastic optimization," *arXiv preprint arXiv:1412.6980*, 2014.

[16] T.-Y. Lin, M. Maire, S. Belongie, J. Hays, P. Perona, D. Ramanan, P. Dollár, and C. L. Zitnick, "Microsoft coco: Common objects in context," in *European conference on computer vision*. Springer, 2014, pp. 740–755.

[17] http://www.cipr.rpi.edu/resource/stills/index.html, 05/16/2019.

Author Biography

Takahiro Kudo received the B.E. degrees in electrical engineering from Keio University in 2018. He is currently an M.E. student at Keio University under the supervision of Prof. Masaaki Ikehara. His research interests are in the field of applications of image denoising, image deblurring, and machine learning.

Takanori Fujisawa received the B.E., M.E. and PhD degrees in electrical engineering from Keio University in 2014, 2016, and 2019 respectively. He is currently an Post-Docs at Keio University under the supervision of Prof. Masaaki Ikehara. His research interests are in the field of applications of sparse coding to image super resolution, image inpainting, and automatic music transcription.

Takanori Fujisawa received the B.E., M.E. and PhD degrees in electrical engineering from Keio University in 2014, 2016, and 2019 respectively. He is currently an Post-Docs at Keio University under the supervision of Prof. Masaaki Ikehara. His research interests are in the field of applications of sparse coding to image super resolution, image inpainting, and automatic music transcription.

Takuro Yamaguchi received the B.E., M.E. and PhD degrees in electrical engineering from Keio University in 2014, 2016, and 2018 respectively. He is currently an associate professor at Keio University under the supervision of Prof. Masaaki Ikehara. His research interests are in the field of image reconstruction.

Masaaki Ikehara received the B.E., M.E. and PhD degrees in electrical engineering from Keio University in 1984, 1986, and 1989, respectively. He is currently a Full Professor with the Department of Electronics and Electrical Engineering, Keio University. His research interests are in the areas of multi-rate signal processing, wavelet image coding, and filter design problems.

JOIN US AT THE NEXT EI!

IS&T International Symposium on

Electronic Imaging

SCIENCE AND TECHNOLOGY

Imaging across applications . . . Where industry and academia meet!

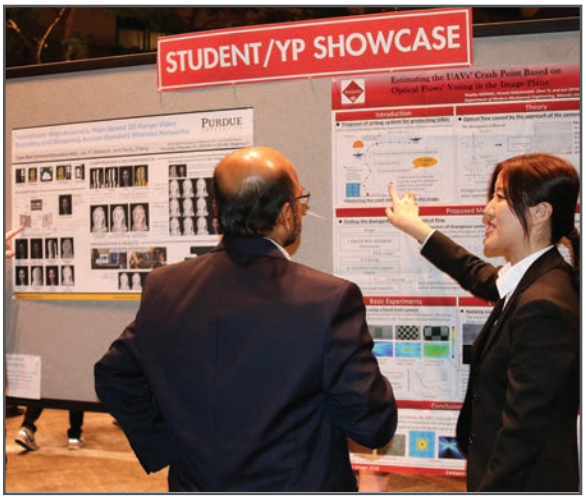

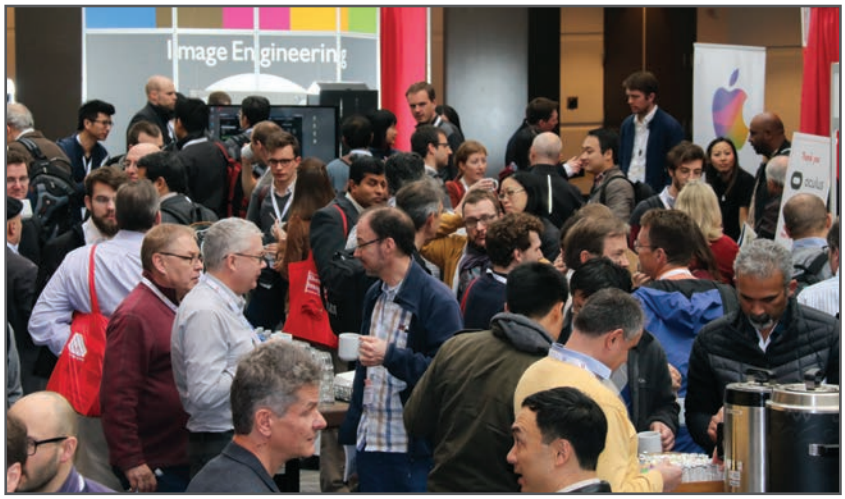

• SHORT COURSES • EXHIBITS • DEMONSTRATION SESSION • PLENARY TALKS •
• INTERACTIVE PAPER SESSION • SPECIAL EVENTS • TECHNICAL SESSIONS •

www.electronicimaging.org

IS&T
imaging.org